Paramagnetic Cupric Ions Ion-Exchanged into TAPO-5 and TAPO-11 Molecular Sieves

Bo Young Kim, Jong-Sung Yu,* and Chul Wee Lee†

Department of Chemistry, Hannam University, 133 Ojung-dong, Taejon, Korea
†Solid State Chemistry Lab, KRICT, P.O. Box 107, Yusung, Taejon 305-606, Korea
Received September 6, 1999

Titaniumaluminophosphate molecular sieves TAPO-5 and TAPO-11 have been hydrothermally synthesized. These materials were characterized using XRD, TGA, BET, ICP, diffuse reflectance UV-Vis and IR techniques. Especially, infrared and diffuse reflectance UV-Vis spectroscopic measurements were made in order to determine the evidence for framework substitution of Ti into $AlPO_4$ materials. The calcined TAPO-5 and TAPO-11 molecular sieves were ion-exchanged with cupric nitrate solution. The location and interactions of cupric ions ion-exchanged into H-TAPO-5 and H-TAPO-11 molecular sieves with water and ammonia have been studied by electron spin resonance (ESR) and electron spin echo modulation (ESEM) spectroscopies. Similarity and difference in Cu(II) location and coordination were discussed in these two structures. There is a gradual transition upon dehydration of Cu-TAPO-5 from a Cu(II) species with ESR parameters $g_{\|} = 2.401$, $A_{\|} = 155 \times 10^{-4}$ cm^{-1}, and $g_{\perp} = 2.08$ to a Cu(II) species with $g_{\|} = 2.348$, $A_{\|} = 167 \times 10^{-4}$ cm^{-1} and $g_{\perp} = 2.07$. A similar gradual transition upon dehydration of Cu-TAPO-11 was also observed from a Cu(II) species with ESR parameters $g_{\|} = 2.375$, $A_{\|} = 151 \times 10^{-4}$ cm^{-1} and $g_{\perp} = 2.08$ to a Cu(II) species with $g_{\|} = 2.333$, $A_{\|} = 170 \times 10^{-4}$ cm^{-1} and = 2.07. In the hydrated state, Cu(II) ion directly coordinates to three water molecules in Cu-TAPO-5 while to two water molecules in Cu-TAPO-11. Upon dehydration treatments, Cu(II) is suggested to be located in hexagonal prism sites recessed from a main channel for both Cu-TAPO-5 and Cu-TAPO-11. Upon equilibration with ammonia, Cu(II) forms a complex containing four molecules of ammonia for both structures based on resolved nitrogen hyperfine interaction.

Introduction

Porous molecular sieves including zeolites have been the subject of extensive study in recent years in view of their great importance as industrial and laboratory scale catalysts.[1,2] In particular, titanium containing molecular sieves are of current interest in zeolite science with respect to their unique catalytic behaviour.[3] Titanium compounds have been widely used as catalysts in the selective oxidation of various organic substrates. Titanium silicalite (TS-1) is an effective molecular-sieve catalyst for the selective oxidation of alkanes, the hydroxylation of phenol and the epoxidation of alkenes in the presence of H_2O_2.[4-6] Several other new titanium containing molecular sieves have been synthesized including TS-2,[7] Ti-ZSM-48[8] and Ti-β,[9] and been explored for their catalytic activities and their characterization. There is another interesting group of titanium containing molecular sieves called titaniumaluminophosphate (TAPO-n), where titanium is substituted into the frameworks of aluminophosphate ($AlPO_4$-n).[10-13] Ti is substituted for phosphorus atoms in $AlPO_4$-5. For the $AlPO_4$-11 sample, divalent and trivalent metals are substituted for Al^{3+} whereas tetravalent metals (*i.e.* Si^{4+} and Ti^{4+}) are substituted for either P or for Al + P atoms.[12] Thus these TAPO-n molecular sieves can have both ion-exchange capacity and catalytic activity.

In this work, TAPO-5 and TAPO-11 were hydrothermally synthesized and infrared and diffuse reflectance UV-Vis spectroscopic measurements were made in order to determine the evidence for framework substitution of Ti in $AlPO_4$-5 and $AlPO_4$-11. Cu(II) ion is incorporated into TAPO-5 and TAPO-11 by ion-exchange to explore the coordination characteristics of Cu(II) in TAPO-5 and TAPO-11 framework. The interactions of Cu(II) with D_2O and ammonia were monitored by electron spin resonance (ESR) and electron spin echo modulation (ESEM) spectroscopy to deduce the location and coordination geometries of Cu(II) in these two TAPO framework structures. In my best knowledge, Cu(II) ions in the Cu(II)-exchanged TAPO molecular sieves are explored at the molecular level by ESR and ESEM techniques for the first time in this work. Parameters obtained from ESR can be used to deduce the oxidation states and the local symmetry of transition metal ions, and the analysis of ESEM signals yields information about the number of interacting adsorbate nuclei (N), their interaction distance (R), and their weak isotropic hyperfine coupling (A_{iso}).[14-19]

Experimental Section

Synthesis and Exchange Process. TAPO-5 and TAPO-11 were synthesized hydrothermally using synthetic gel mixture based on the literature. TAPO-5 was synthesized on the basis of the method described in European patent.[13] Phosphoric acid (85%, Aldrich), pseudo-bohemite (Vista), titanium isopropoxide (97%, Aldrich), tetrapropylammonium hydroxide (1.0 M solution in water, Aldrich) and deionized water were used to prepare the oxide molar ratio of TPAOH : Al_2O_3 : P_2O_5 : 0.3 TiO_2 : 40 H_2O. The mixture was aged with stirring at room temperature to form a homogeneous gel.

The resulting reaction mixture was placed in a stainless steel pressure vessel lined with Teflon and heated at 150 °C for 264 h without agitation.

TAPO-11 was synthesized on the basis of the method described by Ulgappan and Krishnasamy.[10] Gel mixture was prepared with dipropylamine as templating agent. Gel A was prepared by soaking aluminium isopropoxide (98%, Aldrich) in deionized water. Solution B consisted of deionized water and phosphoric acid (85%, Aldrich), to which titanium tetrabutoxide (97%, Aldrich) was added, followed by addition of hydrogen peroxide (30%, Oriental Chem. In.), which resulted a clear dark orange solution. Solution B was added to gel A, followed by the addition of the appropriate amount of triethylamine (99.99%, Aldrich) and stirred to form a homogeneous gel with the oxide molar ratio of dipropylamine : Al_2O_3 : P_2O_5 : 0.1 TiO_2 : 40 H_2O. The resulting gel was placed in a stainless steel pressure vessel lined with Teflon and heated at 187 °C for 24 h without agitation.

The resulting white solid was washed repeatedly with distilled water, filtered and then dired at room temperature. The structure of the synthesized materials was examined by powder X-ray diffraction (XRD) using a Rigaku diffractometer with Cu K_α radiation. The XRD patterns of the as-synthesized materials agreed with those of $AlPO_4$-5 and $AlPO_4$-11 in the literature.[20-23] Thermogravimetric analysis (TGA) were performed on a Dupont 950 thermogravimetric analyser.

The as-synthesized TAPO materials were then heated in flowing oxygen at 550 °C for 10 h to remove the template. Chemical analysis was performed by a Jarrel-Ash Polyscan 61E inductively coupled plasma spectrometer. The nitrogen BET surface areas were measured on a Micromeritics ASAP 2000 analyser. The chemical compositions of the dehydrated materials determined by inductive coupled plasma (ICP) spectrometer are $H_{0.04}[Al_{0.51}P_{0.47}Ti_{0.02}]O_2$ and $H_{0.07}[Al_{0.53}P_{0.46}Ti_{0.01}]O_2$ for H-TAPO-5 and H-TAPO-11, respectively (see Table 1). The resulting H-TAPO molecular sieves were then partially exchanged at room temperature for 12 h by dropwise addition of 10 mM copper(II) nitrate(Alfa) according to the procedure described in earlier work.[24,25] The samples were then filtered, washed with hot distilled water in order to remove excess Cu(II) ions on the surface of the sample, and dried in air at room temperature to form CuH-TAPO-5 and CuH-TAPO-11[26] with the composition $Cu_{0.012}H_{0.016}[Al_{0.51}P_{0.47}Ti_{0.02}]O_2$ and $Cu_{0.012}H_{0.046}[Al_{0.53}P_{0.46}Ti_{0.01}]O_2$, respectively.

Sample Treatment. The CuH-TAPO sample was loaded directly into a Suprasil quartz ESR tube (2 mm id by 3 mm od) connected to a vacuum and gas handling line. Dehydration of the sample was carried out by first evacuating the sample at room temperature followed by slowly heating to 450 °C over an 12 h period in a static reactor. Following this evacuation the sample was exposed to 200-400 Torr of static high-purity dry oxygen for 6-10 h at 450 °C in order to oxidize any copper species that was reduced during the heating period. Finally, the oxygen was pumped off at room temperature under a 10^{-5} Torr vacuum. This heat treated sample with flowing oxygen is termed a dehydrated sample.

After dehydration, adsorbates as both vapor and gas were admitted at room temperature to the sample tube and left to equilibrate. Adsorbates such as D_2O and $^{15}NH_3$ were obtained from Aldrich and Cambridge Isotope Laboratories, and used after repeated freeze-pump-thaw cycles.

Spectroscopic measurements. Infrared spectroscopic measurements were carried out using a Perkin Elmer Spectrometer. For measurements, the sample diluted with dry KBr was compressed to a wafer with a diameter of about 1 cm and placed directly in the IR beam. UV-VIS diffuse reflectance spectra were measured with Shimadzu UV-2501PC spectrophotometer equipped with a reflectance attachment and $BaSO_4$ was used as a reference material. ESR spectra were measured at 77 K and room temperature on an ESP 300 Bruker spectrometer. ESEM spectra were recorded at 4.5 K with a Bruker ESP 380 pulsed ESR spectrometer. Three pulse echoes were measured by using a 90°-τ-90°-T-90° pulse sequence with the echo measured as a function of T. In a typical ESEM study, the deuterium modulation from a deuterated adsorbate is analysed to determine its coordination to Cu(II) in terms of the number of deuterium nuclei, N, at distance, R, with isotropic hyperfine coupling A_{iso}. For typical data, N is determined to the nearest integer, R to ±0.01 nm and A to ±10%. The time between the first two pulses, τ, is set to maximize the deuterium modulation. Theory and simulation of three pulse ESEM spectra are described elsewhere.[27]

Results and Discussion

Powder XRD measurements were performed before and after calcination of as-synthesized TAPO-5 and TAPO-11 to confirm the synthesized structures. Figures 1(a) and 1(b) show the XRD patterns of as-synthesized TAPO-5 and TAPO-11 samples. The XRD pattern is consistent with those of $AlPO_4$-5 and $AlPO_4$-11 in the literature.[20-23] There was no significant changes in the peak positions before and after calcination. The peak intensity was slightly increased after calcination for TAPO-5, while decreased by about 20 % for TAPO-11.

Figure 2 shows the IR spectra of TAPO-5 and TAPO-11 in the range of 4000-400 cm^{-1}. In general, IR spectra of TAPO are similar to those of $AlPO_4$ and SAPO. But TAPO-5 and

Table 1. Gel and product compositions of TAPO-5 and TAPO-11

Sample	Gel composition[a]			Product composition of calcined sample[b]			Composition of Cu(II) exchanged samples
	x	y	z	a	b	c	
TAPO-5	1	0.3	1	0.51	0.47	0.02	$Cu_{0.012}H_{0.016}[Al_{0.51}P_{0.47}Ti_{0.02}]O_2$
TAPO-11	1	0.1	1	0.53	0.46	0.01	$Cu_{0.012}H_{0.046}[Al_{0.53}P_{0.46}Ti_{0.01}]O_2$

[a]x template: y TiO_2 : z Al_2O_3 : P_2O_5 :40 H_2O TPAOH and DPA were used as templates for TAPO-5 and TAPO-11, respectively. [b]$(Al_aP_bTi_c)O_2$

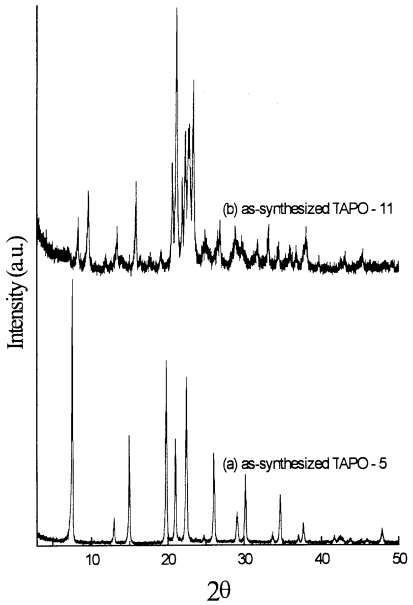

Figure 1. XRD patterns for (a) as-synthesized TAPO-5 and (b) as-synthesized TAPO-11.

TAPO-11 have a weak absorption band near 970-960 cm^{-1} which doesn't appear in IR spectra of corresponding $AlPO_4$ and SAPO molecular sieves. A characteristic absorption at 970-960 cm^{-1} was also observed in the framework IR spectra of titanosilicate-1, which was attributed to the presence of titanium in the tetrahedral Si-O-Ti linkages.[28] Thus the IR band can be interpreted either as a stretching mode of framework Ti(IV) containing units such as $[TiO_4]$ or $[OHTiO_3]$ or as a mixture of the two modes.[29]

Figure 3 shows diffuse reflectance UV-VIS spectra for calcined TAPO-5 and TAPO-11. Absorption is rather broad, but absorption maximum near 230 nm is observed for both

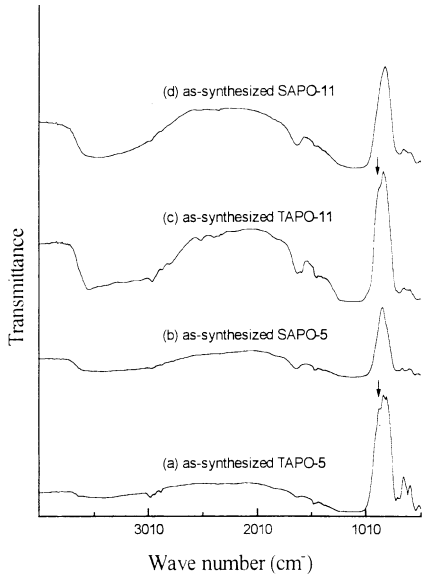

Figure 2. IR spectra of (a) as-synthesized TAPO-5 (b) as-synthesized SAPO-5 (c) as-synthesized TAPO-11 (d) as-synthesized SAPO-11 at room temperature. Absorption band near 970-960 cm^{-1} is marked by an arrow in TAPO-5 and TAPO-11 sample.

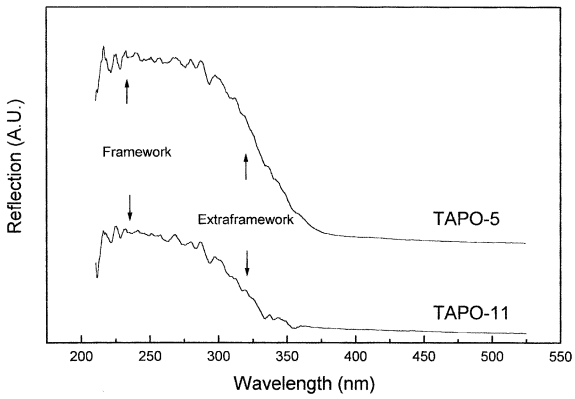

Figure 3. Diffuse reflectance UV-VIS spectra of calcined TAPO-5 and TAPO-11.

TAPO-5 and TAPO-11, which is accepted as evidence of isolated Ti(IV) in the framework position.[30,31] This signal is considered to be due to charge-transfer process in $[TiO_4]$ or $[OHTiO_3]$ units, and thus is directly connected with framework Ti(IV).[30] Absorption is also weakly observed at about 320 nm, which is characteristic for Ti(IV) species in extraframework titania particles. Thus some of titanium species may be also located in extraframework position. Spectral band for rutile, which is usually above 400 nm is not observed in our TAPO samples. As-synthesized TAPO-5 and TAPO-11 also showed almost an identical broad absorption band with about the same intensity ratios at 230 nm and 320 nm to those of calcined samples. This indicates that as-synthesized TAPO samples themselves have extraframework titanium species, and there was no observable extraction of titanium species from framework position during calcination. The ICP data of calcined TAPO-5 and TAPO-11 molecular sieves in Table 1 also support the incorporation of Ti into the framework. The determined chemical composition of the calcined TAPO samples indicates that Ti mainly replaces P rather than Al when incorporated into $AlPO_4$ framework as also suggested by Zahedi-Niaki *et al.*[12] Thus occuring ion-exchange capacity of TAPO materials was confirmed by paramagnetic Cu(II) ESR signal intensity. $AlPO_4$-5 and $AlPO_4$-11, which have a neutral framework showed very weak Cu(II) intensity upon Cu(II) ion exchange. However, TAPO-5 and TAPO-11 showed much stronger ESR Signal (~100 times stronger) as shown below.

The BET surface area of calcined TAPO-5 and TAPO-11 are 385 m^2/g and 138 m^2/g, respectively. These values are mostly consistent with those in the literature.[12] Figure 4 shows the thermogravimetric analysis (TGA) and derivative thermogravimetry (DTG) curves for as-synthesized TAPO-5 and TAPO-11 samples. There are three distinct weight losses at 20-300, 300-450, and 450-800 °C for TAPO-5. The first loss is due to desorption of water, and the second and third losses are assigned to the decomposition of the templates. The second and third loss correspond to 10.0% and 0.6% of total sample weight, respectively. For TAPO-11, two distinct weight losses at 20-200 and 200-500 °C, were observed, which correspond to water desorption and template decomposition.

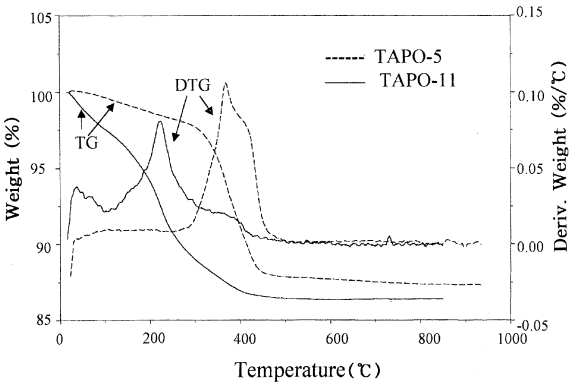

Figure 4. TGA and DTG curves of as-synthesized TAPO-5 and as-synthesized TAPO-11.

After calcination, there was only one weight loss at 20-200 °C corresponding to water desorption for both TAPO structures.

Framework structure and site locations. Figure 5 shows the framework structure of TAPO-5 and TAPO-11 molecular sieves. These structures do not have analogs in zeolite structures. TAPO-5 consists of 4-, 6- and 12-ring channels while TAPO-11 consists of 4-, 6- and 10-ring channels, which are interconnected by 6-ring windows. Figure 5c shows a view looking down the c-axis into the 10-ring with an elliptical cross section of 0.62×0.39 nm.[32] The dashed lines at the borders of the 10-ring represent 6-ring edges in the faces of the 10-ring channel which are probable positions for cation location by analogy to cation locations in zeolites in TAPO-11 framework. The 6-ring locations are denoted as site II by analogy to the 6-ring locations in zeolites.[24,25] Notice that there are two different II positions in the TAPO-11 materials which are denoted as II_1 and II_2. The II position corresponds to a position in the plane of three oxygens in the 6-ring window whereas II* corresponds to displacement from that position out towards the 10-ring and II' corresponds to displacement of that position back into the 6-ring. This is shown more clearly in Figure 5b. Also note that site I is in the center of a double 6-ring and site U is in the center of a 10-ring. Site I' is in the plane of the O_3 oxygens of the 6-ring.

In TAPO-5 as shown in Figure 5a the structure is somewhat different in that only one type of site II exists which corresponds to the II_2 position in TAPO-11. The other sites are the same as in TAPO-11. TAPO-5 has a 12-ring main channel with a circular cross section of 0.73×0.73 nm.[32]

Electron spin resonance and Electron spin echo modulation. X-ray diffraction analysis can be employed to determine the location of cations.[33] All of the TAPO molecular sieves have very low framework negative charge[20] (also see Table 1). So only a small amount of Cu(II) ions are exchanged. This is typically at the limits of X-ray analysis. However, ESR and ESEM techniques can be used to determine the location of paramagnetic cations even though present in very low concentration.[14-19] ESR signals are useful for identification of the local geometry and oxidation state of transition metal ions. The Cu(II) ESR spectral measurements at 77 K of Cu-TAPO-5 before and after various evacuation treatments are shown in Figure 6. A fresh hydrated sample

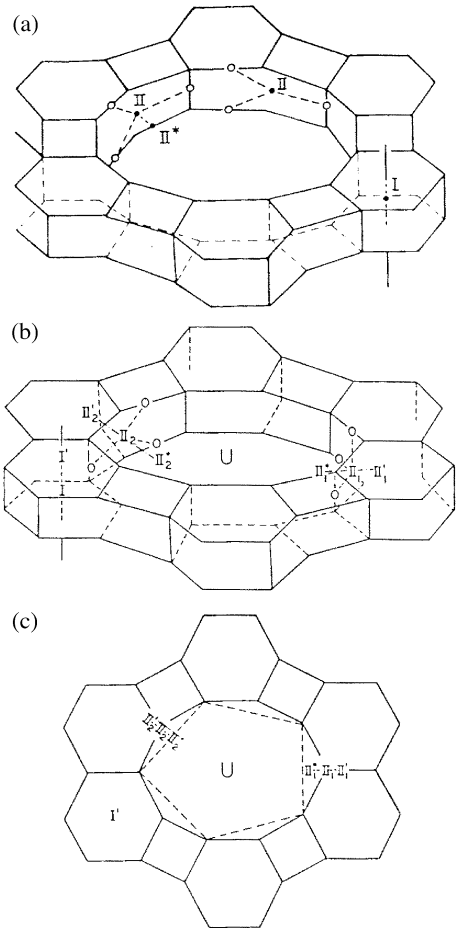

Figure 5. Simplified framework structures of TAPO-5 and TAPO-11. The smallest and next smallest rings are 4-rings and 6-rings, respectively, While the large ring is an elliptical 10-ring in TAPO-11 and a circular 12-ring in TAPO-5. (a) TAPO-5 structure, (b) TAPO-11 structure and (c) view along the large central ring channel axis of TAPO-11 where the dashed lines show edges of 6-ring windows that form the surface of a 10-ring channel.

before evacuation produces predominantly one species with ESR parameters of $g_{\|} = 2.401$ and $A_{\|} = 155 \times 10^{-4}$ cm^{-1} characteristic of an axial powder spectrum of Cu(II) as shown in Figure 6a. The hyperfine lines of the perpendicular component are not resolved. A value of $g_{\perp} = 2.08$ was estimated for the perpendicular component of the g tensor. An almost identical anisotropic ESR spectrum is observed when measured at room temperature. The ESR parameters are consistent with octahedral geometry for the Cu(II) ions.[14,15] When the sample is evacuated at room temperature followed by higher temperature, the $g_{\|}$ value decreases while $A_{\|}$ coupling gradually increases. Figure 6b shows the ESR spectrum of fresh sample measured at 77 K after evacuation at 260 °C for 10 h. A new species occurs, which has ESR parameters of $g_{\|} = 2.346$, $A_{\|} = 168 \times 10^{-4}$ cm^{-1} and $g_{\perp} = 2.07$. The Cu(II) ESR intensity was decreased to about 12% of fresh sample, based on double integration of the total Cu(II) intensities. This indicates the decrease of Cu(II) spin concentration because Cu(II) is thermally reduced to Cu(I) during evacuation. Further evacuation for a longer period and at higher temperature

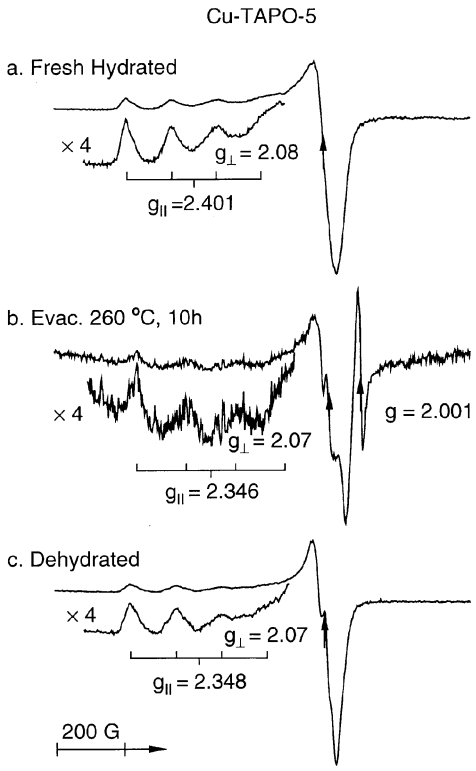

Figure 6. ESR spectra at 77 K of Cu-TAPO-5 (a) in fresh hydrated state, (b) evacuated at 260 °C for 10h and (c) dehydrated by evacuation at 450 °C for 10 h, oxidation with dry oxygen at 450 °C for 5-10 h, and then evacuation at room temperature for 20 min.

didn't change the g values of the signal. The second species is the only Cu(II) species observed for evacuation at 450 °C. But the intensity of Cu(II) signal was decreased due to further thermal reduction of Cu(II). 200 Torr of oxygen was added into the evacuated samples, and the sample with added oxygen was heated to 450 °C and maintained there for 8-12 h in order to reoxidize any copper species reduced during evacuation. After evacuation of oxygen at room temperature, the ESR spectrum recovers most of its intensity and shows the same Cu(II) species as that in Figure 6b, with ESR parameters of $g_{\|} = 2.348$, $A_{\|} = 167 \times 10^{-4}$ cm^{-1} and $g_\perp = 2.07$ as shown in Figure 6c.

Figure 7 shows the ESR spectra of Cu(II) at 77 K in a fresh hydrated Cu-TAPO-11 before and after evacuation. In a fresh hydrated TAPO-11 sample, one species is observed with ESR parameters of $g_{\|}$ =2.375, $A_{\|}$ =151×10^{-4} cm^{-1} and $g_\perp$ =2.08 as shown in Figure 7a. A similar anisotropic ESR spectrum is also observed at room temperature. When Cu-TAPO-11 is evacuated at increasing temperature, a similar trend in the ESR spectra to that for Cu-TAPO-5 is observed with a gradual transition upon dehydration from a species with ESR parameters of the fresh hydrated sample to another new species with ESR parameters of $g_{\|}$ =2.333, $A_{\|}$ =170 × 10^{-4} cm^{-1} and $g_\perp$=2.07 as shown in Figure 7b. Upon dehydration, the ESR spectrum also produces the same second Cu(II) species with Cu(II) ESR intensity fully recovered. When 100 Torr of oxygen gas was adsorbed into dehydrated Cu-TAPO-5 and Cu-TAPO-11 samples, the $A_{\|}$ lines of the

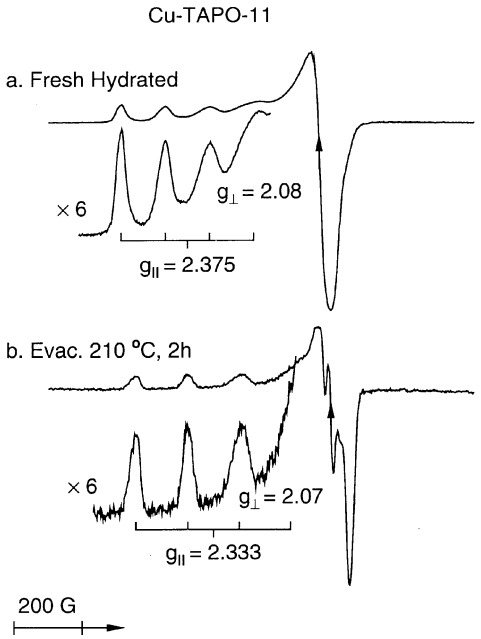

Figure 7. ESR spectra at 77 K of Cu-TAPO-11 (a) in fresh hydrated state and (b) evacuated at 210 °C for 2h.

Cu(II) species were not broadened by adsorbed O_2. This indicates that the Cu(II) ions in dehydrated state are located at recessed sites which oxygen cannot enter.[16-19] Table 2 summarizes the ESR parameters of Cu-TAPO-5 and Cu-TAPO-11 after various sample treatments.

When dehydrated Cu-TAPO-5 and Cu-TAPO-11 samples are rehydrated by exposure to the vapor pressure of water at room temperature, the original Cu(II) species as shown in the ESR spectra in fresh hydrated samples of Figure 6a and Figure 7a were regenerated from Cu(II) species in dehydrated state, respectively. Three pulse ESEM spectra recorded at 4.5 K and the simulation parameters for Cu(II) in dehydrated Cu-TAPO-5 and Cu-TAPO-11 samples fully rehydrated with D_2O, each of which has almost the same ESR spectrum as a fresh hydrated sample are shown in Figure 8. All ESEM spectra were recorded with the time between the first two pulses set to maximize the deuterium modulation at the magnetic field corresponding to the g spectral region of the Cu(II) powder spectrum. Deuterium modulation from D_2O is clearly observed with a period of about 450 ns. The deuterium modulation is further confirmed by Fourier transformation of these signals. The simulation, shown by broken

Table 2. ESR parameters at 77 K of Cu(II) in Cu-TAPO-5 and Cu-TAPO-11 after various sample treatments

Treatment	Cu-TAPO-5			Cu-TAPO-11		
	$g_{\|}$ [a]	$A_{\|}$ [b]	$g_\perp$ [c]	$g_{\|}$ [a]	$A_{\|}$ [b]	$g_\perp$ [c]
Fresh hydrated	2.401	155	2.08	2.375	151	2.08
Dehydrated	2.348	167	2.07	2.333	170	2.07
+ D_2O	2.398	157	2.08	2.371	151	2.08
+ NH_3	2.241	192	2.044	2.230	187	2.041

[a]Estimated uncertainty is ±0.005. [b]The unit of $A_{\|}$ is 1×10^{-4} cm^{-1} and the estimated uncertainty is $\pm 7 \times 10^{-4}$ cm^{-1}. [c]Estimated uncertainty is ±0.01.

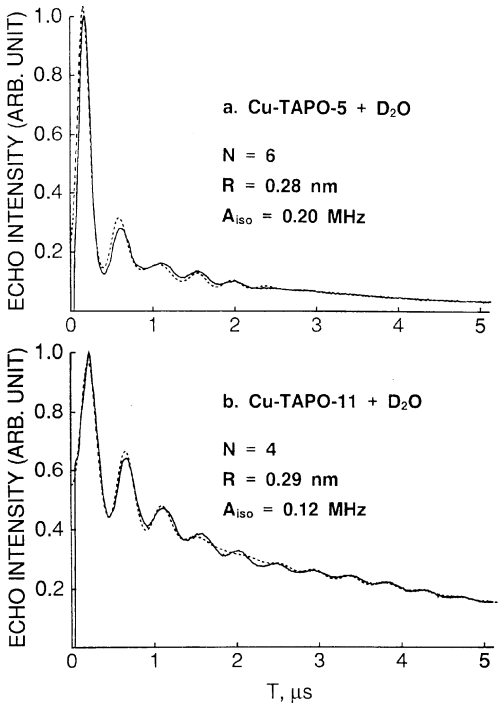

Figure 8. Experimental (——) and simulated (-----) three-pulse ESEM spectra at 4.5 K of fully rehydrated (a) Cu-TAPO-5 and (b) Cu-TAPO-11 with D_2O.

lines, indicates that Cu(II) interacts with six neighboring deuterium nuclei, *i.e*. three water molecules, with a Cu(II)-D distance of 0.28 nm for Cu-TAPO-5.

Interestingly, the deuterium modulation shown in Cu-TAPO-11 in Figure 8b is not as deep as that in Cu-TAPO-5. The best simulation of the ESEM signal for Cu-TAPO-11 indicates that Cu(II) interacts with four deuterium nuclei, *i.e*. two water molecules, with a Cu(II)-D distance of 0.29 nm.

The probable Cu(II) location can be determined on the basis of the ESR and ESEM observations for the Cu(II) species in connection with characteristics of TAPO framework. ESEM result shows that three water molecules situate at a distance of 0.28 nm from a Cu(II) for Cu-TAPO-5. ESR results indicates that the waters directly coordinate with the Cu(II) and the Cu(II) ion has an octahedral environment. From the TAPO-5 structure, only sites I and site II* permit octahedral geometry. Of site I and II*, the former is not reasonable because Cu(II) ion would directly coordinate with six framework oxygens at that site. Site II* is the only possibility left, and a Cu(II) ion at this site is able to coordinates directly with three oxygens from water molecules and three oxygens form six-ring window, thus forming a octahedral configuration as shown in Figure 9. In the case of Cu-TAPO-11, Cu(II) coordinates only to two water molecules based on ESEM results although there are enough room in the channel for coordination to more than two water molecules. Considering lower coordination of Cu(II) in Cu-TAPO-11 compared to Cu(II) in Cu-TAPO-5, we think that sites II^*_1 and II^*_2 are not both populated after incorporation of the cupric ion by ion exchange. Note that site II_1 is in a more constrained environment than site II_2. Because of the differences

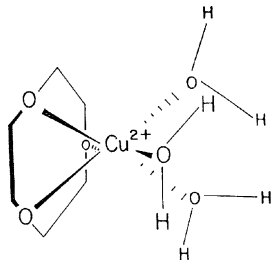

Figure 9. Schematic diagram of a Cu^{2+} ion, located at site II* in an octahedral environment in TAPO-5, directly coordinating to three framework oxygens and three water molecules.

between the results in TAPO-5 and TAPO-11, we conclude that the cupric ion must be in different locations in these two TAPO materials. Thus, since the II_1 site is unique to TAPO-11, we suggest that it is the site preferably occupied by cupric ion In hydrated TAPO-11, coordinating to two water molecules as shown in Figure 10. In TAPO-5 there is only one type of II site which corresponds to the II_2 site in TAPO-11. Deviation of the g values and hyperfine coupling between the fresh and the dehydrated samples suggests that water significantly varies the local environment of the Cu(II) ions. Cu(II) often migrates into coordination sites, which can compensate its lost coordination when losing the coordinated water molecules during dehydration process. Hexagonal prism site, where Cu(II) forms distorted octahedral coordination with six framework oxygens, three above and three below the Cu(II), is electrostatically the most stable and thus is generally the most favored site for exchanged transition metal ions.[15-19,] In TAPO-5 and TAPO-11 structure, site I corresponds to the center of hexagonal prism recessed from a main channel. We conclude that Cu(II) ions in dehydrated state are also located in hexagonal prism sites. In these cases, Cu(II) moves into

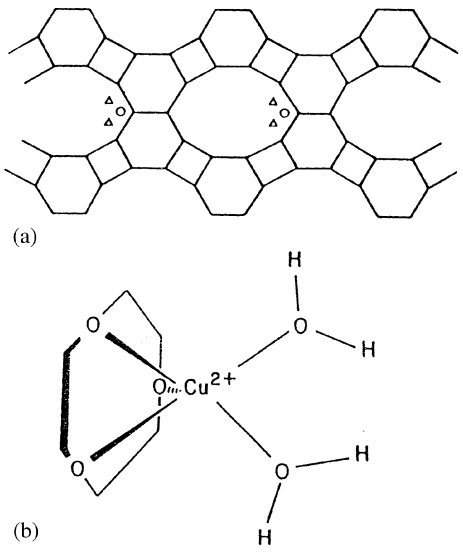

Figure 10. Schematic representation for Cu^{2+} coordinated to water in H-TAPO-11, showing two directly coordinated water molecules in one 10-ring channel and three lattice oxygen atoms from the six-ring window around Cu^{2+}, giving a five-coordinate complex, where the positions of Cu^{2+} ions (○) and water (△); (b) detailed view of the geometry. From ESEM data, the Cu^{2+}-H distance is 0.29 nm.

hexagonal prism sites from the site II* or II_1* in the main channel during dehydration process. This assignment is further supported by a lack of oxygen broadening.

Figure 11 shows ESR spectrum at 77 K of a dehydrated Cu-TAPO-11 after adsorption of 30 Torr of ammonia. A new cupric ion species is observed with ESR parameters of $g_{\|}$ = 2.230 and $A_{\|}$ =187 × 10^{-4} cm^{-1}. Cu-TAPO-11 with adsorbed $^{15}NH_3$ (^{15}N has a nuclear spin of 1/2) show five ^{15}N hyperfine lines centered at g=2.042 and splitted by 21 × 10^{-4} cm^{-1} which are also shown in the expanded second derivative spectrum in the bottom of Figure 11. The intensity ratio of the five ^{15}N hyperfine signals is close to the expected ratio of 1 : 4 : 6 : 4 : 1 for interaction with four nitrogens. With adsorbed NH_3 (^{14}N has a nuclear spin of 1) the ESR spectrum shows nine hyperfine lines in the $g_{\perp}$ region, but they are not resolved clearly (not shown). It can be assigned to the coupling of four equivalent N atoms, indicating that the complex is $[Cu(NH_3)_4]^{2+}$. Tetracoordinated cupric complexes such as CuX_4 (X=Cl, NH_3, etc.) generally prefer a square planar configuration.[34] The ESR parameters are consistent with those of other tetraammonia complexes of Cu(II) with square planar configuration.[35-45] Thus the Cu(II) is suggested to be located at site U, the center of the double ten ring, coordinating to four molecules of NH_3 (see Figure 12). The hydrogen from ammonia can form hydrogen bond to framework oxygens. The ESR spectrum also show a development of a similar new Cu(II) species with ESR parameters of $g_{\|}$ =2.241 and $A_{\|}$ =192 × 10^{-4} cm^{-1} upon adsorption of NH_3 onto dehydrated Cu-TAPO-5. Cu-TAPO-5 with adsorbed $^{15}NH_3$ also show five ^{15}N hyperfine lines centered at g=2.047 and splitted by 20 × 10^{-4} cm^{-1} like in Cu-TAPO-5 (figure not shown). In this case, Cu(II) also forms a square planar configuration with four ammonia molecules. Table 3 summarize the ESR parameters of tetraammonia complexes formed between Cu(II) and ammonia in various zeolites and molecular sieves for comparison.

Paramagnetic Cu(II) species were also characterized un

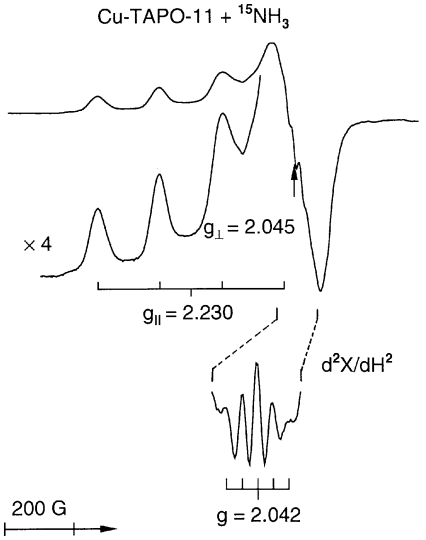

Figure 11. ESR spectrum at 77 K of Cu-TAPO-11 after adsorption of 30 Torr of $^{15}NH_3$ at room temperature.

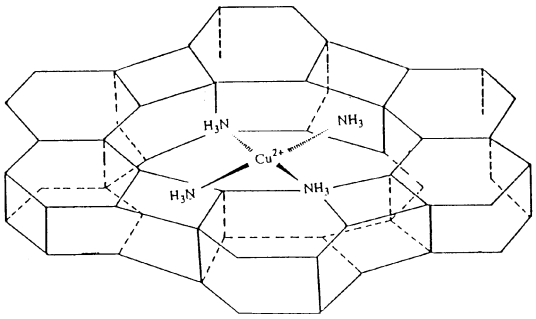

Figure 12. Representation for Cu^{2+} coordinated to four molecules of ammonia in Cu-TAPO-11.

Cu(II)-exchanged SAPO-5 and SAPO-11 by ESR and ESEM.[42,46,47] In general, these results are similar to those in Cu-TAPO-5 and Cu-TAPO-11. But there are also some interesting differences. The anisotropic line shapes of Cu(II) in both SAPO and TAPO materials correspond to Cu(II) ions subject to an axial crystal field. The observed magnetic parameters of Cu(II) was rather different to each other between Cu-TAPO-5 and Cu-SAPO-5 and between Cu-TAPO-11 and Cu-SAPO-11. There was also interesting differences in the change of Cu(II) ESR intensities during evacuation for dehydration. ESR spectra continue to lose its Cu(II) ESR intensities during evacuation at increasing temperature in Cu-TAPO samples (2-3% of Cu(II) concentration in hydrated Cu-TAPO for evacuation at 450 °C), while maintained about 20-30% of Cu(II) in hydrated Cu-SAPO for the identical processes. Similar dehydration behaviors were observed in aluminosilicate L and gallosilicate L molecular sieves.[37,38] But trends of magnetic parameters were similar during dehydration process; *i.e.* $g_{\|}$ values slightly decreased and $A_{\|}$ values increased. The adsorbate interactions of Cu(II) with H_2O and ammonia were also similar to each other between Cu-TAPO-n and corresponding Cu-SAPO-n. Cu(II) coordinates with 3 water molecules in Cu-TAPO-5 and Cu-SAPO-5 while 2 water mol-

Table 3. ESR parameters at 77 k of tetraammonia complexes of Cu(II), $[Cu(NH_3)_4]^{2+}$ with square planar symmetry in various molecular sieves. "ch" represents a channel-type zeolite and "ca" represents a cage-type zeolite. The values 1.3 and 1.2 nm are the internal diameters of α-cage

Matrix	$g_{\|}$ [a]	$A_{\|}$ [b]	Type:size	Reference
TAPO-5	2.241	192	ch:12-ring	this work
TAPO-11	2.230	187	ch:10-ring	this work
AlMCM-41	2.281	170	ch:39 nm	35
Siliceous MCM-41	2.289	178	ch:43 nm	36
K-L gallosilicate	2.254	175	ch:12-ring	37
K-L aluminosilicate	2.255	177	ch:12-ring	38
ZSM-5	2.246	183	ch:12-ring	39-41
SAPO-11	2.226	190	ch:10-ring	42
X zeolite	2.228	178	ca:1.3 nm	43
Y zeolite	2.235	175	ca:1.3 nm	44
rho	2.239	175	ca:1.2 nm	45

[a]Estimated uncertainty is ±0.008. [b]The unit of $A_{\|}$ is 1·10^{-4} cm^{-1} and the estimated uncertainty is ±7 × 10^{-4} cm^{-1}. [c]SAPO-11 represents silicoaluminophosphate molecular sieves.

ecules in Cu-TAPO-11 and Cu-SAPO-11. Cu(II) also forms a square planar tetraammonia complex in both Cu-TAPO-11 and Cu-SAPO-11. But Cu(II) coordinates only with three ammonia molecules in Cu-SAPO-5 while with four ammonia molecules in Cu-TAPO-5. These new structural results are relevant to Ti and Cu(II) catalyzed reactions in TAPO molecular sieves.

Conclusions

TAPO-5 and TAPO-11 were synthesized hydrothermally and confirmed by a X-ray diffraction. IR, diffuse reflectance UV-Vis and ESR spectra indicate that Ti ions mostly incorporate into tetrahedral framework sites in TAPO-5 and TAPO-11. It was found that Ti atoms are mainly substituted for P atoms in these two structures. Cu(II) ion was incorporated into TAPO-5 and TAPO-11 by ion-exchange to explore the coordination characteristics of Cu(II) in TAPO-5 and TAPO-11 framework for the first time. ESR and ESEM data indicate that Cu(II) is initially located in a main channel coordinating to water molecules in hydrated states and then migrated into the hexagonal prism of the structures during dehydration process. Cu(II) is located in a more recessed site, which is unique in TAPO-11 coordinating to two water molecules, while to three water molecules in Cu-TAPO-5. Cu(II) forms distorted octahedral coordination with six framework oxygens, three above and three below the Cu(II) in the center of the hexagonal prism upon dehydration. When polar adsorbates are adsorbed on dehydrated samples, Cu(II) migrates back to a main channel where Cu(II) can coordinate with adsorbates. When water is adsorbed on the dehydrated samples, the original Cu(II) species in hydrated TAPO samples is regenerated with Cu(II) coordinating to water molecules in the main channel. Upon adsorption of ammonia, Cu(II) forms a tetraammonia complex with a square planar configuration in the main channel.

Acknowledgment. The authors wish to acknowledge the financial support of the Korean Research Foundation made in the program year of 1997, and thank Taejon Korea Basic Science Institute for the elemental analysis by ICP. The authors are also grateful to Prof. Larry Kevan at the Department of Chemistry in University of Houston for ESEM measurements.

References

1. Thomas, J. M.; Theocharis, C. R. In *Modern Synthetic Methods*; Scheffold, R., Ed.; 1989; Vol. 5, p 249.
2. Thomas, J. M. In *Intercalation Chemistry*; Whittingham, M. S., Jacobson, A. J., Eds.; 1982; p 55.
3. Sheldon, R. A. *Top. Curr. Chem.* **1993**, *164*, 21.
4. Taramasso, M.; Perego, G.; Notari, B. *US Patent* No. 4410501, 1983.
5. Huybrechts, D. R. C.; Bruycker, L. De; Jacobs, P. A. *Nature* **1990**, *345*, 240.
6. Notari, B. In *Structure-Activity and Selectivity Relationships in Heterogeneous Catalysis*; Grasselli, R. K., Sleight, A. W., Eds.; 1991; p 243.
7. Reddy, J. S.; Kumar, R.; Ratnasamy, P. *Appl .Catal.* **1990**, *58*, L1.
8. Serrano, D. P.; Li, H. X.; Davis, M. E. *J. Chem. Soc., Chem. Commun.* **1992**, 745.
9. Camblor, M. A.; Corma, A.; Martinez, A.; Perez-pariente, J. *J. Chem. Soc., Chem. Commun.* **1992**, 589.
10. Ulagappan, N.; Krishnasamy, V. *J. Chem. Soc., Chem. Commun.* **1995**, 373.
11. Thomas, J. M.; Whittingham, M. S.; Jacobson, A. J. In *Intercalation Chemistry*; 1982; p 55.
12. Zahedi-Niaki, M. H.; Joshi, P. N.; Kaliaquine, S. *Studies in Surface Science and Catalysis* **1997**, *105*, 1013.
13. *European Patent* No. 121232, 1984.
14. Dyrek, K.; Che, M. *Chem. Rev.* **1997**, *97*, 305.
15. Kevan, L. *Acc. Chem. Res.* **1987**, *20*, 1.
16. Yu, J.-S.; Ryoo, J. W.; Kim, S. J.; Hong, S. B.; Kevan, L. *J. Phys. Chem.* **1996**, *100*, 12624.
17. Yu, J.-S.; Ryoo, J. W.; Lee, C. W.; Kim, S. J.; Hong, S. B.; Kevan, L. *J. Chem. Soc., Faraday Trans.* **1997**, *93*, 1225.
18. Yu, J.-S.; Kim, J. Y.; Lee, C. W.; Kim, S. J.; Hong, S. B.; Kevan, L. *J. Chem. Soc., Faraday Trans.* **1997**, *93*, 4211.
19. Yu, J.-S.; Kim, J. Y. *Catal. Today* **1998**, *44*, 81.
20. Flanigen, E. M.; Lok, B. N.; Patton, L.; Wilson, S. T. *Pure Appl. Chem.* **1986**, *58*, 1351.
21. Szostak, R. *Molecular Sieves*: *Principles of Synthesis and Identification*; Van Nostrand Reinhold: New York, 1989; Chapter 4.
22. Wilson, S. T.; Lok, B. M.; Flanigen, E. H. *US Patent* No. 4310440, 1982.
23. Wilson, S. T.; Lok, B. M.; Messina, C. A.; Cannan, T. R.; Flanigen, E. M. *J. Am. Chem. Soc.* **1982**, *104*, 1146.
24. Yu, J.-S.; Kevan, L. *J. Phys. Chem.* **1990**, *94*, 7620.
25. Yu, J.-S.; Kevan, L. *J. Phys. Chem.* **1991**, *95*, 3262.
26. Cu-TAPO-n is used to represent CuH-TAPO-n in this work.
27. Kevan, L. In *Time Domain Electron Spin Resonance*; Kevan, L., Schwartz, R. N., Eds.; Wiley-Interscience: New York, 1978; Chapter 8.
28. Nogami, M.; Moviya, Y. *Yogyo-Kyokaishi* **1977**, 59.
29. Camblor, A. M.; Corma, A.; Pirez-pariente, J. *J. Chem. Soc., Chem. Commun.* **1993**, 557.
30. Geobaldo, F.; Bordiga, S.; Zecchina, A.; Giamello, E.; Leofanti, G.; Petrini, G. *Catal. Lett.* **1992**, *16*, 109.
31. Vayssilov, G. N. *Catal. Rev. - Sci. Eng.* **1997**, *39*, 209.
32. Meier, W. M.; Olson, D. H. In *Atlas of Zeolite Structure Types*; Butterworths: London, 1987.
33. Gallezots, P. *Catal. Rev. Sci. Eng.* **1979**, *20*, 121.
34. Purcell, K. F.; Kolts, J. C. *Inorganic Chemistry*; Philadelphia: Saunders, 1977; Chapter 9.
35. Kim, J. Y.; Yu, J.-S.; Kevan, L. *Mol. Phys.* **1998**, *95*, 989.
36. Poppl, A.; Newhhouse, M.; Kevan, L. *J. Phys. Chem.* **1995**, *99*, 10019.
37. Yu, J.-S.; Hong, S. B.; Kevan, L. *Appl. Magn. Reson.* **1996**, *10*, 575.
38. Yu, J.-S.; Kevan, L. *J. Phys. Chem.* **1994**, *98*, 12436.
39. Sass, C. E.; Kevan, L. *J. Phys. Chem.* **1988**, *92*, 5192.
40. Anderson, M. W.; Kevan, L. *J. Phys. Chem.* **1987**, *91*, 4174.
41. Sendoda, Y.; Ono, Y. *Zeolites* **1986**, *6*, 209.
42. Lee, C. W.; Chen, X.; Kevan, L. *J. Phys. Chem.* **1992**, *96*, 357.
43. Gallezot, P.; Ben Taarit, Y.; Imelik, B. *J. Catal.* **1972**, *26*, 295.
44. Bereman, R. D.; Kosman, D. J. *J. Am. Chem. Soc.* **1977**, *99*, 7322.
45. Anderson, M. A.; Kevan, L. *J. Phys. Chem.* **1987**, *91*, 2926.
46. Lee, C. W.; Chen, X.; Kevan, L. *J. Phys. Chem.* **1991**, *95*, 8626.
47. Chen, X.; Kevan, L. *J. Am. Chem. Soc.* **1991**, *113*, 2861.